Icarus 217 (2012) 462–473

Contents lists available at SciVerse ScienceDirect

Icarus

journal homepage: www.elsevier.com/locate/icarus

Aerial electromagnetic sounding of the lithosphere of Venus

Robert E. Grimm [a,*], Amy C. Barr [a], Keith P. Harrison [a], David E. Stillman [a], Kerry L. Neal [b], Michael A. Vincent [b], Gregory T. Delory [c]

[a] Dept. of Space Studies, Southwest Research Institute, 1050 Walnut St. #300, Boulder, CO 80302, United States
[b] Dept. of Space Operations, Southwest Research Institute, 1050 Walnut St. #300, Boulder, CO 80302, United States
[c] Space Sciences Laboratory, University of California, 7 Gauss Way, Berkeley, CA 94720, United States

ARTICLE INFO

Article history:
Available online 10 August 2011

Keywords:
Venus, Interior
Lightning
Geophysics
Thermal histories
Ionospheres

ABSTRACT

Electromagnetic (EM) investigation depths are larger on Venus than Earth due to the dearth of water in rocks, in spite of higher temperatures. Whistlers detected by Venus Express proved that lightning is present, so the Schumann resonances ~10–40 Hz may provide a global source of electromagnetic energy that penetrates ~10–100 km. Electrical conductivity will be sensitive at these depths to temperature structure and hence thermal lithospheric thickness. Using 1D analytic and 2D numerical models, we demonstrate that the Schumann resonances—transverse EM waves in the ground-ionosphere waveguide—remain sensitive at all altitudes to the properties of the boundaries. This is in marked contrast to other EM methods in which sensitivity to the ground falls off sharply with altitude. We develop a 1D analytical model for aerial EM sounding that treats the electrical properties of the subsurface (thermal gradient, water content, and presence of conductive crust) and ionosphere, and the effects of both random errors and biases that can influence the measurements. We initially consider specified 1D lithospheric thicknesses 100–500 km, but we turn to 2D convection models with Newtonian temperature-dependent viscosity to provide representative vertical and lateral temperature variations. We invert for the conductivity-depth structure and then temperature gradient. For a dry Venus, we find that the error on temperature gradient obtained from any single local measurement is ~100%—perhaps enough to distinguish "thick" vs. "thin" lithospheres. When averaging over thousands of kilometers, however, the standard deviation of the recovered thermal gradient is within the natural variability of the convection models, <25%. A "wet" interior (hundreds of ppm H_2O) limits EM sounding depths using the Schumann resonances to <20 km, and errors are too large to estimate lithospheric properties. A 30-km conductive crust has little influence on the dry-interior models because the Schumann penetration depths are significantly larger. We conclude that EM sounding of the interior of Venus is feasible from a 55-km high balloon. Lithospheric thickness can be measured if the upper-mantle water content is low. If H_2O at hundreds of ppm is present, the deeper, temperature-sensitive structure is screened, but the "wet" nature of the upper mantle, as well as structure of the upper crust, is revealed.

1. Introduction

The geodynamic style of a solid planet or satellite is controlled by the thickness of its lithosphere, or strong, comparatively cold, outer shell. The coherent part is formally the mechanical lithosphere, whereas the thermal lithosphere is the (generally thicker) conductive boundary layer to internal solid-state convection. We treat the thermal lithosphere in this paper, and denote its maximum and mean thicknesses as L and $\bar{L}$, respectively.

Earth's lithosphere has been globally investigated through earthquake seismology, with additional contributions from other geophysical methods. $\bar{L} = 100$ km for oceanic lithosphere and $\bar{L} = 200$ km for continental lithosphere (Schubert et al., 2001). Solid-state convection in the Earth has a freely moving lithosphere 100 km thick—plate tectonics—because temperature-dependent viscosity contrasts are modest (Solomatov, 1995), probably moderated by the presence of water.

The unknown mean thickness and variability of the lithosphere of Venus are major obstacles to characterizing its geodynamic style. The best constraints at present come from the correlation between gravity and topography, which indicates apparent depths of Airy isostatic compensation of 150–350 km for spherical harmonic degrees 3–10 (Sjogren et al., 1997). Local correlations, expressed alternatively as geoid-to-topography ratio (GTR), indicate Pratt compensation depths of 140–400 km for the volcanic rises, with an average value around 260 km (Moore and Schubert, 1997). The Pratt compensation depth is equivalent to L.

* Corresponding author. Fax: +1 303 546 9687.
E-mail address: grimm@boulder.swri.edu (R.E. Grimm).

0019-1035/$ - see front matter © 2011 Elsevier Inc. All rights reserved.
doi:10.1016/j.icarus.2011.07.021

A lithospheric thickness significantly greater than Earth's is not consistent with heat flow scaled from Earth or from chondritic meteorites. Purely conductive equilibrium with terrestrial heat sources would lead to $\overline{L} = 40$—45 km, too thin to support large-scale topography (Solomon and Head, 1982; Turcotte, 1995). Parameterized-convection models using chondritic heat sources and a free upper boundary (or small viscosity contrast) produce about three-quarters of the current terrestrial flux after 4 billion years (Phillips and Malin, 1983; Solomatov and Moresi, 1996) so, scaling from oceanic lithosphere, $\overline{L} < 150$ km for a "plate-tectonic" Venus. (Also, Kaula and Phillips (1981) derived $\overline{L} = 94$ km directly from thermal-boundary layer theory using terrestrial heat flux.) Yet there is no evidence for contemporary lithospheric recycling in the geological record of Venus (Solomon et al., 1992). If indeed $\overline{L} = 200$—300 km and Venus has a chondritic or terrestrial complement of radionuclides, then "Venus cannot presently be in an approximate thermal steady state" (Schubert et al., 1997).

Numerical models of mantle convection suggest that strongly temperature-dependent viscosity leads to such large contrasts that the lithosphere becomes stationary (Solomatov and Moresi, 1996). Such "stagnant-lid" convection could be a consequence of a dearth of water. Imposition of a stagnant lid 0.6–2 byr ago in parameterized-convection models reduces current heat flow to as low as 30% of the value just prior to stagnation (Solomatov and Moresi, 1996; Phillips et al., 1997). The stagnant lid cools while the deeper interior heats up—an evolution away from equilibrium that has been postulated to trigger episodic lithospheric foundering and global resurfacing (Turcotte, 1993).

The harsh surface conditions of Venus and large resource requirements pose serious challenges to a network of long-lived geophysical stations that might further probe the lithosphere in accustomed ways. Seismic coupling to the dense atmosphere of Venus could be detectable as ionospheric perturbations, thus enabling seismology from orbit (Lognonné et al., 2005). A satellite constellation is necessary, however, for optimum implementation. Another way to exploit the dense atmosphere for subsurface investigation is to perform electromagnetic sounding from a balloon in the relatively benign environment near 55-km altitude. Balloons are a component of the Venus Flagship concept definition (Bullock et al., 2009) and have been considered by others for Discovery (NASA) or Cosmic-Vision (ESA) class missions (Wilson et al., 2011). The pioneering VEGA balloons lasted a few days (Sagdeev et al., 1986), but balloon longevity can potentially be measured in circumnavigations.

We present a series of numerical and analytical models to demonstrate the feasibility of aerial electromagnetic sounding on Venus, specifically to determine lithospheric thickness—the pivotal geodynamic parameter. The relevant natural sources are discussed, and how the unique properties of the ground-ionosphere waveguide enable high-altitude EM sounding. Measurement errors are incorporated and a new high-performance sensor configuration is proposed. Subsurface temperature profiles are specified or are taken from numerical models of mantle convection. Temperature-dependent electrical conductivity of the ground is calculated from laboratory measurements of either dry or "wet" olivine. The ionospheric conductivity is also considered. Particular attention is given to the effects of ionospheric variability on the inference of ground conductivity, as boundary coupling in effect generates a joint ionosphere-subsurface inverse problem.

2. Electromagnetic sounding

2.1. Earth–Venus comparison

Electromagnetic (EM) sounding encompasses a wide variety of methods used to sense subsurface structure from less than a few meters to a thousand kilometers or more (see Telford et al., 1990; Simpson and Bahr, 2005; Grimm, 2009, for reviews). Below 1 Hz, abundant natural energy exists on Earth from magnetospheric pulsations and from the interaction of the magnetosphere with diurnal heating of the ionosphere. Above 1 Hz, the ground-ionosphere waveguide allows lightning energy to be recorded globally as the 8–34 Hz Schumann resonances and regionally as higher frequency impulses.

The fundamental parameter controlling EM exploration is the skin depth δ (km) = $0.5\sqrt{\rho_a/f}$ (e.g., Telford et al., 1990), where ρ_a is the apparent resistivity (Ω m) of the ground and f is the frequency (Hz). The apparent resistivity is the resistivity of a half-space that is equivalent to the (depth-dependent) ground under test. We drop the subscript for convenience and allow all resistivities to be apparent values unless otherwise noted, such as for specific material properties. The exploration depth

$$D\ (\mathrm{km}) = 0.36\sqrt{\rho/f} \tag{1}$$

is a better representation of depths at which true resistivity can be recovered (e.g., McNeill, 1990) and figures directly in the asymptotic inversion used here (Section 3.6).

We compare subsurface electrical resistivity on Earth and Venus and implications for EM sounding in Fig. 1. Representative resistivity-depth profiles for Earth follow Egbert and Booker (1992) and Lizarralde et al. (1995). The Venus profiles were constructed by specifying temperature vs. depth and then laboratory conductivity-temperature measurements were used to form resistivity vs. depth (Section 3.2). The lower resistivity of the terrestrial lithosphere and upper asthenosphere, even compared to the Venus

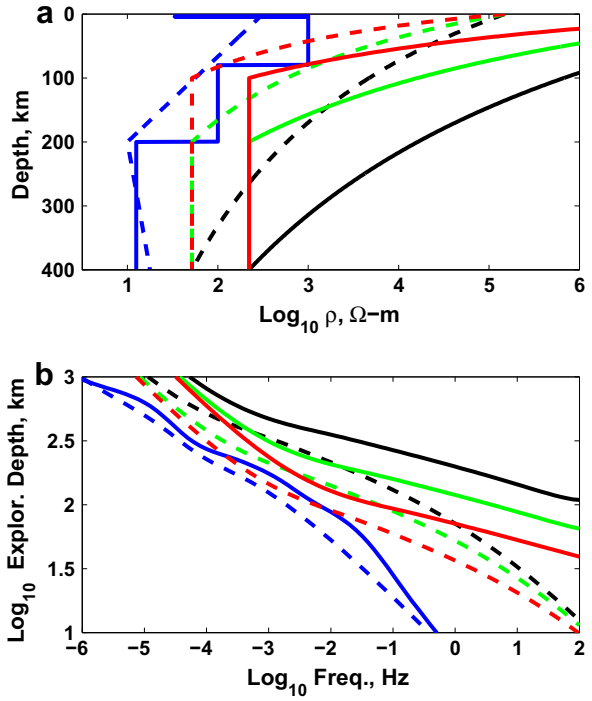

Fig. 1. (a) Comparison of electrical resistivity on Earth and Venus. Blue: Earth structure (dashed: smoothed model of Egbert and Booker (1992); solid: layered model of Lizarralde et al. (1995)). Remaining curves are Venus: solid, dry; dashed, wet (~200–600 ppm H_2O). Black, green, red: lithospheric thicknesses of 400, 200, and 100 km, respectively. (b) Comparison of electromagnetic (EM) investigation depths. Increase in resistivity due to dry rocks on Venus more than offsets decrease in resistivity due to temperature, so that effective penetration depths are much larger on Venus. This enables sounding of the upper mantle by lightning-caused Schumann resonances at ~10–40 Hz. (For interpretation of the references to color in this figure legend, the reader is referred to the web version of this article.)

"wet" (hundreds of ppm H_2O) profiles, is likely due to aqueous fluids and/or graphite films (e.g., Yoshino et al., 2009).

We calculated the apparent resistivity of a layered halfspace using a classical recursion procedure (Wait, 1970; see application in Grimm, 2002). This approach includes both diffusion and propagation; the latter was disabled here for clarity. The frequency-dependent exploration depth then follows readily. (The reader will now note that we switch between conductivity and resistivity in this paper. They are of course reciprocal quantities: geophysicists often prefer resistivity due to its dimensional relation to impedance, whereas physicists use conductivity as the proportionality constant between electric field and current density. However, only resistivity is treated as an apparent or halfspace-equivalent value).

Typical Earth resistivities of 1–100 Ω m can require frequencies $<10^{-5}$ Hz (i.e., periods of days) to penetrate hundreds of kilometers (Fig. 1). Such measurements have been useful in characterizing the lithosphere, asthenosphere, and mantle transition zone, but can be very challenging to make. Even exploration to tens of kilometers depth calls for frequencies in the millihertz range, which still need long, stationary, ground measurements. For Venus, however, the presumed dearth of water makes resistivities much higher and hence allows for deeper exploration (Fig. 1). At 10 Hz, for example, D can be up to 130 km. Venus-analog materials that approach 1 MΩ m imply exploration depths 100 times greater than Earth at the same frequency. Alternatively, the same depth can be sounded at a frequency 10^4 times higher than on Earth.

This is the first enabling factor for EM exploration of the subsurface of Venus: the crust and upper mantle can be probed >1 Hz instead of ≪1 Hz as for Earth. This has several benefits. It allows specific sources (Section 2.2) and propagation properties (Section 2.3) to be exploited. All EM measurements will enjoy higher signal-to-noise ratio (SNR) due to integration of more cycles in a specified time. Most importantly, electric fields can be measured capacitively, because impedance decreases in direct proportion to frequency.

2.2. EM sources: lightning detection on Venus and the Schumann resonances

Venus lacks the geomagnetic-band (<1 Hz) magnetospheric-pulsation and ionospheric-dynamo signals that are all-important to deep EM exploration on Earth, but this does not matter because of the frequency shift expected for the relatively dry interior. The spheric band (>1 Hz) is so named on Earth because it is dominated by "radio atmospherics," a variety of signals due to lightning discharges. Impulsive signals at several kHz to MHz are useful to understand the lightning source, but have unfavorable geometrical properties for high-altitude EM sounding (Section 2.3). These signals are probably propagative in the venusian subsurface (loss tangent ≪1) and penetrate just the top few kilometers.

The nearly continuous lightning discharge rate on Earth ($\sim$100 s^{-1}) globally fills the ground-ionosphere waveguide and sets up longitudinal normal modes, the Schumann resonances (see Nickolaenko and Hayakawa, 2002, for a review). Each mode contains an integral multiple of wavelengths around the planet: an ideal spherical cavity (vacuum between perfect boundary conductors) has eigenfrequencies

$$f_m = \frac{c}{2\pi a}\sqrt{m(m+1)} \quad (2)$$

where c is the speed of light in vacuum, $m = 1, 2, 3, \ldots$, and a is the planetary radius. Earth's readily measured Schumanns lie at 8, 14, 20, 26, and 32 Hz, which are lower than predicted for the ideal cavity due to conduction losses. The quality factor Q measures the ability to sustain propagation in the face of conduction losses into the ground or ionosphere. Nickolaenko and Hayakawa (2002) show that Q is the ratio of the waveguide thickness to the skin depth in the boundary conductor(s). For Earth, the skin depth in the ground (or ocean) is negligible and $Q = 4$–8 over the first four frequencies due to ionospheric losses.

Several groups have studied the likely properties of Schumann resonances on Venus (Nickolaenko and Rabinowicz, 1982; Pechony and Price, 2004; Simões et al., 2008). Ideal-waveguide frequencies differ only by the ratio of planetary radii, i.e., the fundamental eigenfrequency would lie at 11 Hz. Ionospheric conductivity lowers the fundamental to 9 Hz with estimates of Q from 5 to 10 for this mode. Simões et al. (2008) also modeled a lossy lower boundary, i.e., finite ground conductivity. They adopted a model temperature profile from Arkani-Hamed (1994) but simply chose conductivity measurements for "silicon oxide" and for felsic rocks, neither of which is appropriate for a nearly anhydrous, mafic, venusian crust and upper mantle. Simões and co-workers considered an alternative model with conductivity reduced by a factor of 100, but these high- and low-conductivity profiles are still about a factor of 100 more conductive than our models (Section 3.2) using "wet" and dry olivine, respectively. The fundamental eigenfrequency in their joint ionosphere-ground model falls to 8 Hz and $Q = 4$. The eigenfrequencies and quality factors could both be lower if the higher resistivities used here were adopted.

Evidence for lightning on Venus—the necessary source for the Schumann resonances—has been debated for nearly three decades (see Grebowsky et al., 1997, for a review). We view the recent measurements from the Venus Express (VEX) vector magnetometer as definitive evidence for lightning. Russell et al. (2007) reported bursts of field-aligned, circularly-polarized energy near the spacecraft periapsis. This is a diagnostic signature of a whistler wave that is vertically refracted through the ionosphere as it traverses from below. Whistlers are uniquely associated with lightning because the dispersion arises from an impulsive source (the actual dispersion cannot be observed by VEX due to bandwidth limitation). Russell et al. (2008) refined the estimate of flash rate to 18 s^{-1}, about 20% of Earth's. The amplitudes are, however, unknown. The Schumann excitation is proportional to the current moment, or current times (return) stroke length (see Nickolaenko and Hayakawa, 2002). R strokes per second contribute an amplitude multiplier between $\sqrt{R}$ and R, depending on whether the signals add incoherently or coherently, respectively. Thus the estimated difference in flash rate will multiply the Venus Schumann amplitudes by 0.2–0.4. This could be offset by larger peak currents or longer stroke lengths on Venus. The cloud-to-ground distance, for example, is an order of magnitude larger on Venus. Without any other information, we will assume an Earth-like 300 μV/m for the vertical electric field and 1 pT for the horizontal magnetic field. It is also worth noting that at lower flash rates the TEM excitation may appear as discrete pulses, akin to terrestrial Q-bursts, instead of a continuous harmonic signal.

This is the second enabling factor for EM exploration of the subsurface of Venus: abundant natural energy, in the form of lightning-caused Schumann resonances, is very likely to exist in the desired exploration bandwidth.

2.3. The ground-ionosphere waveguide

Although the Schumann resonances are the result of normal modes in a spherical shell, they can be described locally and approximately as transverse electromagnetic (TEM) modes, with neither electric nor magnetic fields in the propagation direction. For a wave propagating horizontally in the x-direction, the electric field is vertical (E_z) and the magnetic field is horizontal and orthogonal to propagation (flux density B_y: for discussion purposes, we neglect the formal right-hand convention of the Poynting vector that would orient positive B in the negative y direction). In an ideal

waveguide, the boundaries are nodes and so the TEM wave can exist at all frequencies where no more than one-half free-space wavelength exists across the vertical extent of the waveguide, i.e., up to ~2 kHz on Earth for the ~70-km effective waveguide height. A variety of transverse magnetic (TM) modes exists above the TEM cutoff, in which waves with no magnetic field in the propagation direction reflect back and forth from the boundaries.

In a waveguide with imperfectly conducting boundaries, the TEM wave acquires a small tilt so that the Poynting vector transmits energy through the boundaries. Hence a small electric field appears in the propagation direction, E_x. This wave tilt W is:

$$W = \left|\frac{E_x}{E_z}\right| = \left|\frac{1}{n}\right| \cong \sqrt{\rho\omega\varepsilon_0} \tag{3}$$

where n is the apparent complex index of refraction of the ground (see McNeill and Labson, 1991, for a review). In turn, $n^2 = \varepsilon_r - i/\rho\omega\varepsilon_0$, where ε_r is the relative permittivity (dielectric constant), ρ is the resistivity, ω is the angular frequency, ε_0 is the permittivity of free space, and $i = \sqrt{-1}$. The dielectric contribution can be neglected at Schumann frequencies, which leads to the approximation in Eq. (3). For the range of Venus conditions shown in Fig. 1, $W = 0.1–2°$. Because $E_z = cB_y$, and again neglecting the dielectric term:

$$\left|\frac{E_x}{B_y}\right| = \sqrt{\rho\omega/\mu_0} \tag{4}$$

where μ_0 is the permittivity of free space. Solving Eq. (3) or (4) for ρ gives the apparent resistivity as a function of frequency, using either the vertical electric field (wave-tilt method, WT) or the horizontal magnetic field (magnetotelluric method, MT) as the reference to which the horizontal electric field is compared.

We have analyzed the sensitivity with altitude for vertically incident, TM, and TEM waves: airborne EM on Earth is carried out at low altitude because of a qualitative understanding that sensitivity falls off with altitude, but this has never been quantified. Vertically incident waves were treated directly by computing the apparent resistivity at altitude z, where the air is simply a zero-conductivity layer. The ground resistivity is correctly recovered for $z \ll D$ (the ground exploration depth, Eq. (1)), but the ground appears as a perfect (informationless) conductor for $z \gg D$. Therefore the theoretical maximum altitude at which vertically incident plane waves can be used is $z = D$.

TM waves were analyzed numerically using the same approach described below (Section 3.4) for TEM waves. Many modes are excited from a compact source and so complicated field patterns appear. The apparent resistivity diverges quickly with altitude from the ground value. Consider, however, that the TM signals, visualized as rays, are "detached" from the boundary over most of their multiple reflected paths due to short wavelengths compared to the waveguide thickness. Heuristically, it is only when they are very near the surface that they "feel" its effect, and so again the maximum altitude at which the subsurface can be sensed is also about an exploration depth in the ground.

TEM waves present a very different geometry for subsurface exploration. We begin with an analytical treatment and present numerical results for Venus below (Section 4.1). We assume that E_z is constant across the waveguide (although it may vary horizontally). Eq. (3) gives the wavetilt at the planetary surface for a ground resistivity ρ_g, and a complementary relation holds at the ionobase for an ionospheric resistivity ρ_i. Therefore $E_{xg} > 0$ and $E_{xi} < 0$ at the boundaries can be calculated: the signs provide the correct senses of wave tilt. The power P dissipated in each of the boundaries is proportional to the vertical integral of E_x^2 in each medium. Because $E_x(z) = E_x(0)e^{-z/\delta}$, it is straightforward to derive $P \propto \delta$. Therefore, $P_i/P_g = \delta_i/\delta_g$. Now the loss into the ionosphere must be drawn from the ionobase down to some "crossover" altitude z_c, and similarly the loss into the ground is drawn from below z_c. From the power ratio,

$$\frac{z_c}{h} = \frac{\delta_g}{\delta_g + \delta_i} = \frac{\sqrt{\rho_g}}{\sqrt{\rho_g} + \sqrt{\rho_i}} \tag{5}$$

where h is the waveguide thickness (ionobase altitude) and the resistivities are still understood to be the apparent values for the respective layered media. The apparent resistivity at any altitude $\rho(z)$ is given by:

$$\sqrt{\rho(z)} = \left|\sqrt{\rho_g} - \frac{z}{h}\left(\sqrt{\rho_g} + \sqrt{\rho_i}\right)\right| \tag{6}$$

Fig. 2 illustrates the 1D variation of $\sqrt{\rho(z)}$ in the ground-ionosphere waveguide: it is a linear function between $+\sqrt{\rho_g}$ and $-\sqrt{\rho_i}$. Therefore TEM sensitivity at any point in the waveguide is a simple function of the boundary properties. This relationship is illustrated with numerical calculations below.

This is the third enabling factor for EM exploration of the subsurface of Venus: TEM waves like the Schumann resonances are sensitive everywhere to the properties of the boundaries. Therefore the subsurface can be probed even from high altitude, unlike vertically incident waves or TM waves. The caveat is that the ionosphere must be treated simultaneously. This is a new approach in exploration geophysics.

3. Methods

3.1. Measurements

We assigned the fundamental Schumann a frequency of 10 Hz for convenience, and assumed that the first four resonances, scaled for an ideal cavity, can be measured. In this paper we do not compute the eigenfrequencies *a priori* using our ground and ionospheric conductivities, but rather focus on the ability to recover subsurface properties over a frequency band likely encompassing the Schumanns. When inverting for lithospheric properties, we assumed that spectral estimation has been performed onboard by cascade decimation (Wight and Bostick, 1980) to sharply reduce data volume, so that complex field quantities at just eight discrete frequencies are returned.

Propagation of errors is key to assessing performance. From Eqs. (3) and (4), the errors σ_ρ on apparent resistivity are related to measurement errors on E and B as (Bevington, 1969):

$$\frac{\sigma_\rho^2}{\rho^2} = 4\left(\frac{\sigma_E^2}{E_x^2} + \frac{\sigma_B^2}{B_y^2}\right) \leftrightarrow 4\left(\frac{\sigma_E^2}{E_x^2} + \frac{\sigma_E^2}{E_z^2}\right) \tag{7}$$

where the first expression is for MT and the second is for WT. The measurement errors for E and B are σ_E and σ_B, respectively. We

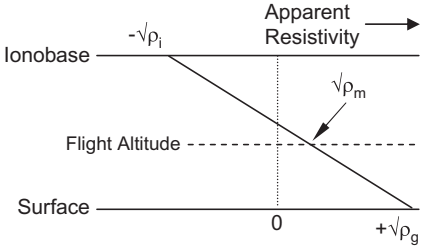

Fig. 2. Square root of measured apparent resistivity ρ_m for TEM waves in ground-ionosphere waveguide is a linear function between the signed square roots of the apparent resistivities of the ionosphere ρ_i and ground ρ_g (see text). The TEM-wave sensitivity does not fall off sharply with altitude, but is sensitive everywhere in the waveguide to the properties of the boundaries.

found it convenient to use the base-10 logarithm of the resistivity, so its error is $\sigma_{\log\rho} = \sigma_\rho/2.718\rho$.

We adopted the following sensitivities for sensors that might be accommodated on a Venus balloon: 0.6 pT for a 20-cm search-coil magnetometer (Roux et al., 2008), 1 μV/m for a nominal double-probe electrometer with horizontal tip separation of 4 m (C. Ferencz, personal communication, 2009), and 0.05 μV/m for a new large electrometer design built into a 6-m balloon hull (see Appendix). The signal-to-noise power (SNR) in the critical horizontal electric-field measurement, $(E_x/\sigma_E)^2$, depends on altitude because E_x is a linear function of altitude. In particular, SNR can degrade near the crossover. We can, however, straightforwardly evaluate the relative benefits of B_y or E_z as the reference measurement. We assume that the vertical electrode separation in the nominal configuration is just 1 m. For an Earth-like 1 pT (300 μV/m) signal, the SNR for B_y is 4 dB but is 37 dB on E_z. If the balloon-hull electrometer is used, SNR = 76 dB on E_z. We conclude that, since an electrometer has to be flown anyway for E_x, it is a better to include an E_z measurement than to fly a separate magnetometer for B_y. For the remainder of this paper we focus on WT measurements, for both the nominal and large electrode configurations.

The very small value of E_x compared to E_z poses a measurement challenge. It is impractical to attempt to keep an aerial platform level or to recover the attitude to <0.1° required to extract E_x: there will be strong cross-contamination from E_z. This problem has been addressed for low-altitude VLF terrestrial surveying as the "quadrature method" (Barringer, 1973; Arcone, 1978). The complex form of Eq. (3) for a uniform halfspace, and neglecting displacement currents, is

$$\frac{E_x}{E_z} = (1+i)\sqrt{\frac{\rho\omega\varepsilon_0}{2}} \tag{8}$$

This indicates that the phase of E_x with respect to E_z is 45° for a uniform halfspace. If the part of the measured E_x that is in quadrature, or out of phase, with E_z, is taken as the inductive signal, then a correction factor of $\sqrt{2}$ will produce the true resistivity from the value inferred solely from the quadrature component. In a halfspace with an arbitrary variation of resistivity with depth, the phase ϕ can vary from 0° to 90° (see Vozoff, 1991). Then the quadrature apparent resistivity is generally defined as

$$\rho_q = \frac{2|W_q|^2}{\omega\varepsilon_0} \tag{9}$$

where W_q is the wavetilt computed from just the quadrature component of E_x. The quadrature apparent resistivity is related to the true apparent resistivity by

$$\rho_q = 2\rho\sin^2\phi \tag{10}$$

For the uniform halfspace, $\phi = 45°$ and $\rho_q = \rho$. Phase increases where a decrease in resistivity is sensed and conversely phase decreases where an increase in resistivity is sensed. Because the phase cannot be measured in the quadrature method, ρ_q may diverge from ρ in non-uniform halfspaces. However, in the case of EM sounding of Venus to depths of tens of kilometers and more, we will rely on a continuous decrease of resistivity with depth due to increasing temperature. Therefore ϕ approaches 90° and $\rho_q = 2\rho$. In other words, almost all of the inductive signal does indeed lie in the quadrature component when resistivity continuously decreases with depth, and so the original definition of ρ (Eq. (3)) can be used, simply taking the quadrature component of E_x relative to E_z. In this way it is not necessary to measure accurately the attitude of the sensors: good results can be obtained as long as the platform is kept, or analytically rotated, to within several degrees of the horizontal.

We incorporated any bias due to the quadrature approximation by treating ρ_q in the resistivity-depth inversions, which was computed using the true ρ and ϕ for a layered medium.

3.2. Subsurface conductivity

The conductivity ς (S/m) as a function of temperature was taken from measurements of dry (Wang et al., 2006) and "wet" (Yoshino et al., 2009) magnesium-rich olivine (~Fo90):

$$\varsigma_{dry} = 250\exp(-1.6/kT) \tag{11}$$

$$\varsigma_{wet} = 79C_w\exp\left[-\left(0.92 - 0.16C_w^{1/3}\right)/kT\right] \tag{12}$$

where k is Boltzmann's constant (8.617×10^{-5} eV/K), T is the temperature (K), and C_w is the water content in weight percent. Eq. (11) closely reproduces earlier results on dry olivine by Constable et al. (1992) at relevant temperatures. The enhancement of solid-state conductivity in silicates by water is actually due to proton diffusion. Other conductivity mechanisms given by Yoshino et al. (2009) can be neglected at high water content. Poe et al. (2010) present alternative results that require less H_2O to yield the same conductivity as Eq. (12). Poe and colleagues suggest differences in FTIR calibration may account for discrepancies in water content. Earth's asthenosphere—defining "wet" for plate tectonics—has up to several hundred ppm H_2O (Bolfan-Casanova, 2005; Karato, 2006). Therefore we adopt 600 ppm in the formula of Yoshino and colleagues (Eq. (12)), equivalent to 220 ppm derived by Poe and coworkers, as representative of a "wet" Venus. Note that Namiki and Solomon (1995) derived a *maximum* of 5 ppm H_2O in the Venus mantle from the inferred hydrogen escape flux and crustal production rate, whereas Grinspoon's (1993) analysis yields the same figure as a *minimum*, when subsequently accounting for degassing of intrusives. Therefore it is likely that Venus lies close to our assumptions for a dry interior.

Two forms were considered for subsurface temperature profiles. In the first, we assumed a constant gradient from 740 to 1690 K across specified L = 100–500 km. These specified lithospheres are useful as starting points for examining effects of parameter variations, and can be considered appropriate as individual or point measurements from a balloon (or descent vehicle). Because a balloon traverse can be measured in tens of thousands of km, however, we are interested in representations of lateral heterogeneity and how well a mean lithospheric thickness can be recovered. To that end we employed numerical models of mantle convection as a second means of setting up temperature profiles.

We used the 2D finite-element, Newtonian temperature-dependent viscosity code CITCOM (Moresi and Solomatov, 1995). The model includes internal heating with a basal (core) component. The mantle was 2900 km thick, the aspect ratio 4:1, and the grid size 23 km. The temperature contrast was 960 K and the viscosity contrast ~10^4. We found that Rayleigh numbers $Ra = 10^2$, 958 (~10^3), and 10^4 corresponded to $\bar{L}$ = 760, 360, and 250 km. The mean lithospheric thickness was measured as the average depth where a linear geotherm fit to the upper mantle meets a constant-fit deep-mantle temperature. Resource limitations prevented further exploration to higher *Ra*, but these models are sufficient for preliminary assessment of EM sounding for a range of $\bar{L}$ that has been inferred for Venus from gravity (Moore and Schubert, 1997) and convection modeling at high *Ra* (Solomatov and Moresi, 1996).

Another option is to include a crust explicitly. We treated the crust as a 30-km thick layer (see Grimm and Hess, 1997, for a review) with conductivity ten times the normal value. Crustal minerals, especially feldspars, have not had the same detailed laboratory measurements under tightly controlled water content as mantle minerals, so there is no good laboratory basis. The crust–mantle

boundary is generally not well-resolved in terrestrial EM surveys due to electrical-equivalence and screening effects of the conductive lower crust. However, very resistive crust can be distinguished as being about a factor of 10 more conductive than the adjacent upper mantle (Jones and Ferguson, 2001).

3.3. Atmospheric and ionospheric conductivity

We fit the profile for scalar conductivity in Fig. 2b of Simões et al. (2008) to the function

$$\log \varsigma_i = \max(0.18z - 26,\ 0.069z - 15.2) \tag{13}$$

where z is the altitude in km. The conductivity is considered well-constrained by data above 120 km altitude, is constructed from theory from zero to 80 km (Borucki et al., 1982), and is interpolated from 80 to 120 km. This function is for the conductivity profile at the subsolar point (solar zenith angle SZA = 0°); Simões and coworkers double the scale height at the antipode (SZA = 180°), which is equivalent to multiplying the z-coefficients by 0.5 in Eq. (13). We took the mean value of [1–½ sin(SZA/2)] over SZA = 0–180°, which multiplies the z-coefficients by 0.682.

We used a suite of numerical models like those described in Section 4.1 to derive the effective altitude of the ionobase and the apparent resistivity of the ionosphere for subsequent analytical calculations. The results are

$$\rho_i = \log f + 4.0, \qquad h = 120 + (f - 10)/2 \tag{14}$$

We considered two sources of error due to the ionosphere: systematic bias and random variations. The former represents an overall uncertainty in the ionospheric scalar conductivity: we take multipliers of ½ and 2, the full SZA scale indicated by Simões et al. (2008). This error moves the ionospheric anchor point in Fig. 2, such that the apparent resistivity measured in the atmosphere projects to an incorrect surface value. The bias is a long-wavelength error, so in addition to global uncertainty it could also represent regional effects like ionospheric holes (should they penetrate to near 120-km altitude). Any variations that have spatial scales similar to or shorter than likely EM integration lengths of tens to hundreds of km can be considered random noise. Relevant ionospheric variations include post-terminator waves and nightside chaos (Brace et al., 1983; Brace and Kliore, 1991). We set the random variations to 50% of the mean ionospheric conductivity.

3.4. Numerical EM methods

The RF package in Comsol Multiphysics version 3.5a was used to calculate propagation of EM fields in a 2D Cartesian lossy waveguide. This is a finite-element code that treats the full Helmholz equation (propagation plus diffusion). The model domain was 1500 km wide and 400 km high, with equal distances above and below the ground surface. The grid size was 2 km. Scattering boundary conditions were used throughout, except for an imposed B_y source on the left-hand boundary. Eq. (13) was applied for the atmospheric–ionospheric conductivity. In later models, a constant-conductivity layer was substituted to represent the ionosphere according to Eq. (14) and the atmospheric conductivity set to zero. Calculated E_x and E_z were exported for postprocessing and the central 1000 km width and altitude 0–120 km extracted for display. This model was used to validate the basic principles of leaky waveguide propagation and to assess lateral resolution and other 2D effects.

3.5. Analytic EM methods

An analytic model was developed to perform the parametric studies of EM sounding that form the bulk of the results in this paper. The apparent resistivity of the ground ρ_g was computed using the Wait (1970) propagator method. The ionospheric apparent resistivity ρ_i followed Eq. (14), then a bias, either double or half of the expected value, was applied. The measured apparent resistivity at altitude was then computed from Eq. (6). The quadrature-measurement bias (Eq. (10)) translated the apparent resistivity to the final, measured value ρ_m. Eq. (6) was again applied to project an inferred ground resistivity from ρ_m and the initially assumed mean ρ_i.

Errors were propagated analytically. The strength of all of the Schumann resonances was assumed to be B_y = 1 pT or equivalently E_z = 300 μV/m (see Section 2.2). Therefore σ_E/E_z (or σ_B/B_y) are constant. E_x is proportional to $\sqrt{\rho}$, so the measured E_x at altitude can also be computed using Eq. (6), which then determines σ_E/E_x. The normalized variance on resistivity due to measurement error (Eq. (7)) was added to the normalized variance of the ionosphere to form a normalized total variance.

3.6. Inversion for resistivity vs. depth

There are a variety of methods used for 1D inversion of apparent resistivity as a function of frequency to true resistivity as a function of depth d in the ground (see Wittall and Oldenburg, 1992, for a review). We used the Bostick (1977) asymptotic inversion, so named because it maps the jth apparent resistivity to the asymptote intersection point of a model with j layers over a half-space. This algorithm is therefore recursive but noniterative, and so was adopted here for simplicity. More robust (Occam) or specialized (D^+) techniques would be used in practice. The appropriate depth multipliers to D in the asymptotic inversion (Wittall and Oldenburg, 1992) were found to be ~0.8.

The analytically propagated error on true resistivity $\sigma_{\rho d}$ is the same as that on apparent resistivity σ_ρ, because of the one-to-one frequency-to-depth mapping. The error on depth $\sigma_d = d[\sigma_\rho/\rho(d)]/2$.

3.7. Inversion for thermal gradient

The resistivity-depth solutions are useful for understanding whether the crust and upper mantle of Venus are wet or dry, and give some qualitative indications of lithospheric thickness. However, terrestrial geophysics has sought to directly link field conductivity-depth and laboratory conductivity-temperature measurements to determine mantle temperature structure (e.g., Constable, 1993; Xu et al., 2000; Yoshino et al., 2009). Here we attempt to recover the lithospheric temperature profile in order to understand the controls on Venus geodynamics, but we allow the parameters of the Ahrennius relationship to be independently estimated. Therefore the recovered resistivity-depth data were fit to a three-parameter model

$$\rho = \rho_0 \exp\left(\frac{A}{R\gamma d}\right) \tag{15}$$

where ρ_0 is the resistivity at the planetary surface, A is the activation energy (kJ/mol), and γ is a linear geotherm (K/km). In practice the logarithm of Eq. (15) was taken for more even weighting, and the least-squares iterative inversion was performed using a subspace-trust method (MATLAB Optimization Toolbox). The error in geothermal gradient σ_γ was determined as

$$\left(\frac{\sigma_\gamma}{\gamma}\right)^2 = \left(\frac{\sigma_f}{\gamma}\right)^2 + \left(\frac{\sigma_d}{d}\right)^2 + \left(\frac{\sigma_{\log\rho}}{\log\rho}\right)^2 \tag{16}$$

where σ_f is the fitting error on γ and the other terms are taken from the resistivity-depth inversion Section 3.6.

4. Results

4.1. Numerical models

We demonstrate the principal behavior of the ground-ionosphere waveguide using a 10-Hz wave (Fig. 3). The altitude-dependent atmospheric–ionospheric conductivity (Eq. (3)) was used. The ground resistivity was set constant at $1 \times 10^6\ \Omega$ m, except for a 100-km patch with 1/10 of this value. These resistivities, while representative of wet and dry olivine in later figures, were chosen simply to assess the lateral resolution and the likely crossover altitude.

First note that the vertical electric field is sharply attenuated near 120-km altitude (Fig. 3a). This is the result of the increase in ionospheric conductivity with altitude, and shows how the waveguide naturally develops when the skin depth in the ionosphere becomes small compared to the waveguide thickness. Note second that the electric field is near-vertical (compare Fig. 3a and b) and that the magnitude of E_z does not vary much vertically across the waveguide. This is the principal feature of a TEM wave that distinguishes it from TM, and also indicates that the atmospheric conductivity is negligible. The change in E_z laterally is due to losses through the boundaries, but this should not be used to compute Q as this is a 2D Cartesian model.

The horizontal E-field (Fig. 3b) changes slowly in general, its magnitude also tracking boundary losses. There is a sharp decrease over the low-resistivity anomaly. E_x varies linearly and changes sign from the surface to the ionobase, confirming Eq. (6). The apparent resistivity (Eq. (3)) shows a continuous decrease with altitude until the null in E_x (dark blue band in Fig. 3c), then increases again above. Comparison of measured apparent resistivity ρ_m to true ground resistivity ρ_g (Fig. 3d) also confirms that lateral heterogeneity is tracked from altitude. Smearing occurs over a lateral extent of about one skin depth, which is exactly what is expected in ground-based surveys (Vozoff, 1991). In the analytical models below, as in a real experiment, the measured apparent resistivity and an estimate of the ionospheric apparent are used to recover the true ground resistivity.

The second numerical model (Fig. 4) simplifies the treatment of the atmosphere and ionosphere but introduces additional lateral heterogeneity into the ionosphere and the ground. The atmosphere was taken to be a layer of zero conductivity from the surface to 120 km altitude. The ionosphere was treated as a uniform layer above, with apparent resistivity varying from 2×10^5 (left) to 1×10^5 (right) Ω m. This is comparable to the full variation with

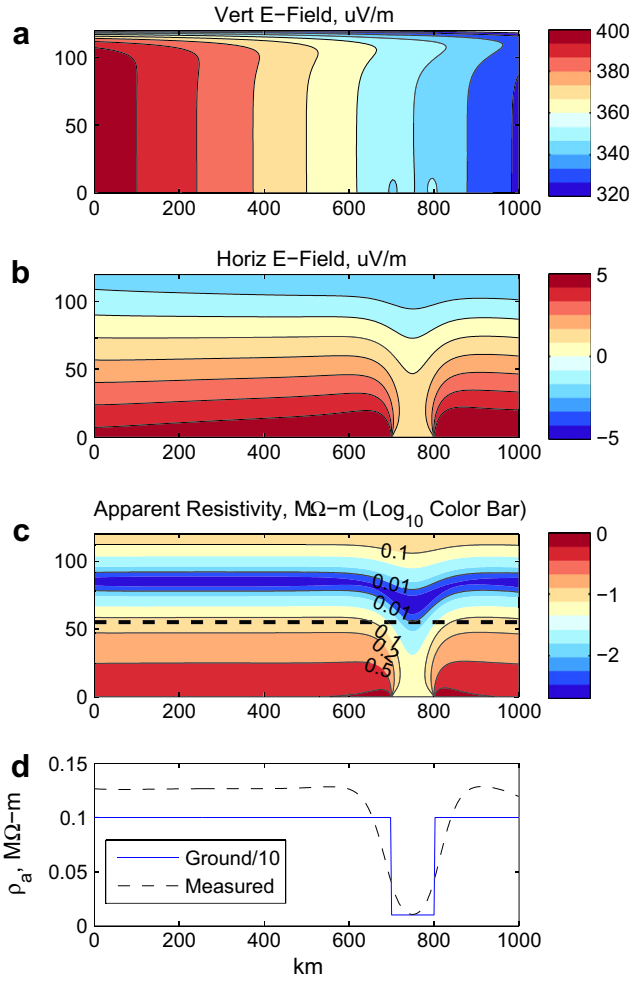

Fig. 3. Numerical model of 10-Hz EM propagation in ground-ionosphere waveguide of Venus (2D Cartesian approximation). Solar-zenith-angle-averaged atmosphere–ionosphere conductivity profile of Simões et al. (2008) naturally develops ionobase (waveguide thickness) at ~120 km altitude (a). Horizontal E-field E_x (b) is much smaller and indicates energy lost through the boundaries ($E_x > 0$ exits into the ground). Apparent resistivity (c) is minimized at the E_x sign change ("crossover") but tracks lateral changes in ground resistivity ((d) 100-km wide arbitrary anomaly). Horizontal resolution is comparable to skin depth in the ground. Dashed line in third panel indicates balloon altitude.

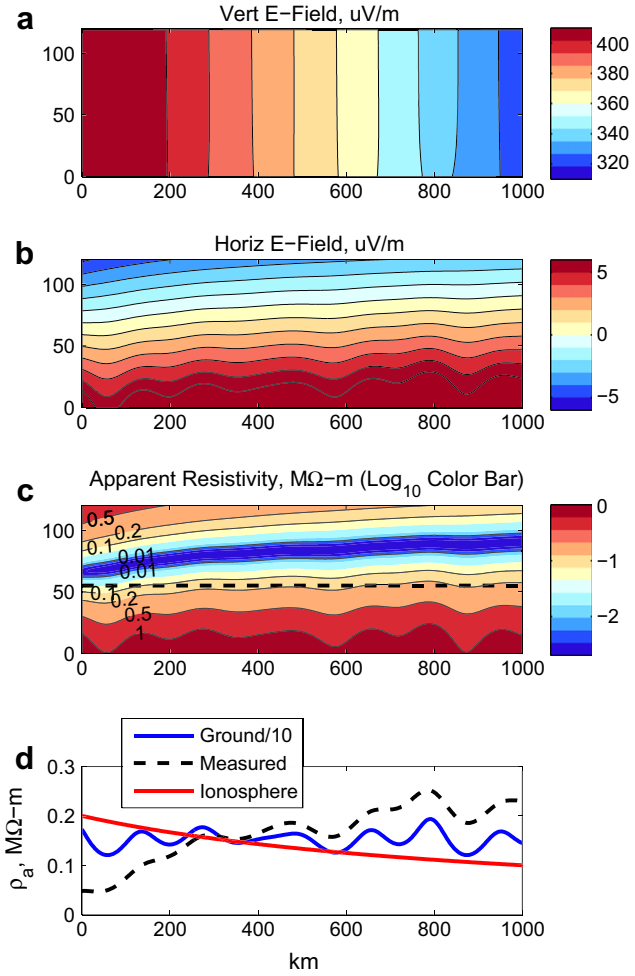

Fig. 4. Numerical model with ionosphere explicitly represented as a conductive layer above 120 km, now illustrating effect of lateral changes in ionosphere and more complex ground properties. Both are laterally compressed for illustration: variation in ionosphere as a function of solar zenith angle 180° at left to 0° at right (Simões et al., 2008; 20,000 km), and variations in $Ra \sim 10^3$ mantle convection model (12,000 km). As ionosphere becomes more conductive, crossover altitude increases, and measured resistivity is more sensitive to the ground.

SZA suggested by Simões et al. (2008), but squeezed horizontally into 1000 km for illustration. Similarly, the apparent resistivity across 10,000 km of convection model at $Ra \sim 10^3$ was computed using the dry olivine law and squeezed into the 1000-km horizontal extent of the displayed EM model. The results are qualitatively similar to the previous model. The electric field is still very nearly vertical, but some deflection is evident in both the vertically changing strength of E_z (Fig. 4a) and the variability in E_x (Fig. 4b). The altitude of the E_x crossover and ρ_m minimum (Fig. 4c) increases from left to right because ionospheric resistivity is decreasing (Fig. 4d), pulling the ionospheric anchor point (Fig. 2) closer to zero. The measurement is everywhere below the crossover in this example, but the apparent resistivity is seen to reflect the properties of both the ground and the ionosphere (Fig. 4d).

These numerical models confirm the analytic derivation that measurements of TEM waves from balloon altitude on Venus are sensitive to the properties of both the ionosphere and the subsurface, with the altitude variation a simple function of the boundary properties. The 2D models also show that lateral resolution is <100 km, a sufficiently long distance to allow signal integration within a resolution element, but small compared with surface scales of mantle convection.

4.2. Analytical models

The effects of a crust and mantle water on conductivity and the aerial measurement procedure to recovering lithospheric thickness were tested using the analytical model described above.

Reference models with specified $L = 100$–500 km (linear temperature gradients), for wet and dry olivine conductivity, are shown in Fig. 5. The asymptotic depth mapping of the first four Schumann resonances onto these resistivity structures are shown as symbols. With no biases, the recovered resistivities match the true resistivities. The ellipses show representative measurement errors using the nominal electrometer. Errors are small for dry olivine because E_x is large at high resistivity, and lithospheric thickness appears to be adequately resolved (this is formalized below as estimated thermal gradient and errors). Conversely, the low resistivity of the wet olivine decreases $(E_x/\sigma_E)^2$ to the point where lithospheric thickness is not well-resolved.

The reference case is hardly changed by inclusion of a 30-km thick, conductive crust (Fig. 6). The Schumann resonances generally penetrate to much greater depths in the dry cases and so are insensitive to the crust. If the lithosphere is as thin as 100 km there is some distortion. The dry-olivine resistivities are still sufficiently high that errors are not affected. The errors compound for wet olivine, but this is immaterial because L cannot be recovered anyway. Note that this modeled wet, conductive crust for Venus is only now moving into the realm of poorly conducting rocks on Earth.

Aerial soundings, including random variations and bias of the ionosphere as well the quadrature bias, are shown in Fig. 7. Two inversions (sets of symbols) are indicated for each specified lithosphere, with the ionospheric resistivity double and half the expected value. These resistivities therefore fall on opposite sides of the true resistivity curves. For dry olivine, the bias suggests that L can still be reasonably estimated. However, the decrease in E_x with altitude now also decreases $(E_x/\sigma_E)^2$, and the ionospheric random errors also contribute, so that the accuracy on L degrades. The measurement accuracy improves the estimate of L when the large electrometer is introduced (dotted ellipses). Biases in the wet-olivine cases strongly shift the recovered curves or even cause the resistivity to diverge from a monotonic decrease with depth. The random errors have also increased.

These tests were repeated using results extracted from the numerical models of mantle convection. The added value is an estimate of the variability about a mean lithospheric thickness $\bar{L}$. Fig. 8

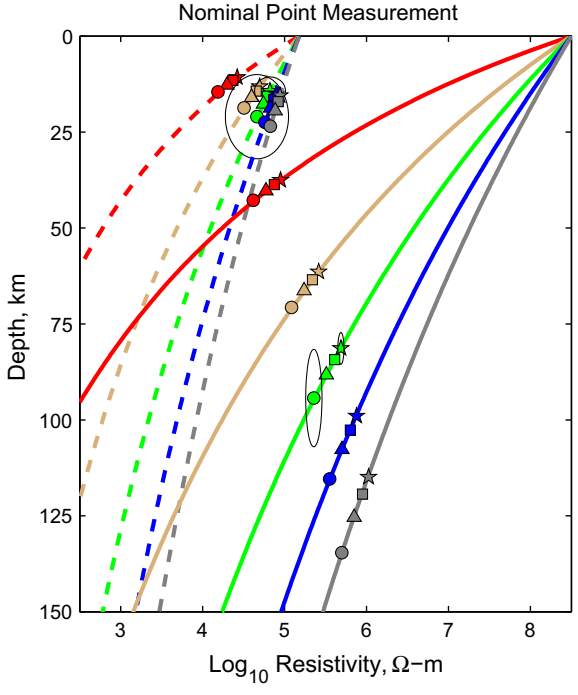

Fig. 5. Dry (solid) and "wet" (dashed) electrical resistivity vs. depth for specified lithospheric thicknesses of $L = 100$–500 km at 100-km increments (red through gray, respectively). Symbols show resistivity structure inverted at the first four Schumann resonances (~10 to ~32 Hz; lowest frequency penetrates deepest). Error ellipses at representative $L = 300$ km and 1st and 4th resonances indicate effect of nominal instrumental errors on resistivity-depth recovery. Random errors are larger for wet resistivity due to smaller induced fields. These calculations represent point measurements without horizontal averaging. (For interpretation of the references to color in this figure legend, the reader is referred to the web version of this article.)

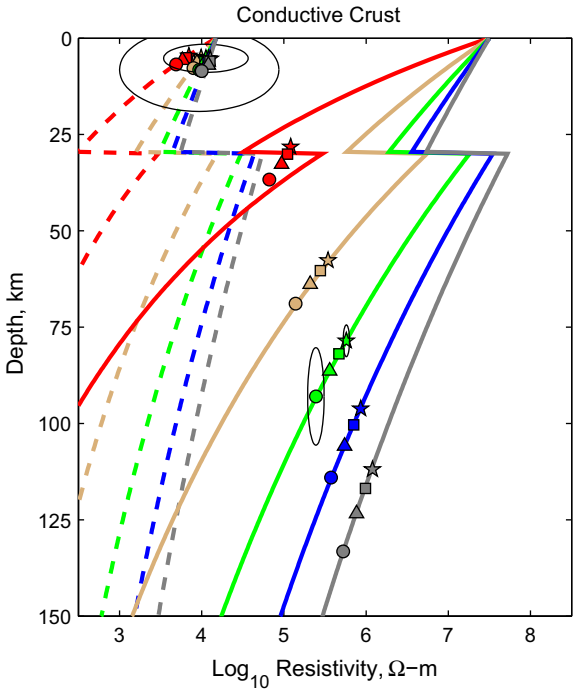

Fig. 6. Effect of electrically conductive 30-km crust on EM point inversion. Systematic error occurs only where Schumann depth sensitivity smears crust–mantle boundary. Random errors remain modest for dry resistivity, but degrade further for wet resistivity.

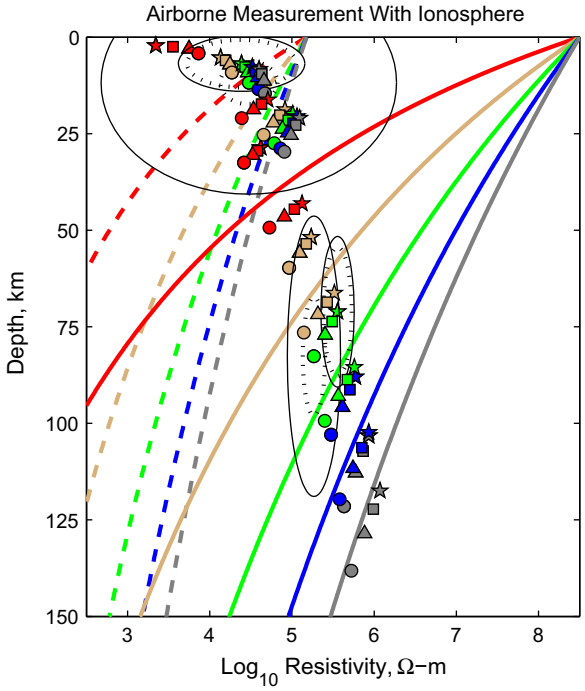

Fig. 7. Effect of airborne measurement on EM inversion. This model includes bias multipliers of ½ and 2 in the noon-to-midnight ionospheric resistivity as well as a 50% local random variation. There are two inversions (sets of symbols) for each curve to cover the bias range. Random errors increase due to the smaller induced fields measured at the balloon altitude (see text). Finally, only the quadrature component is used to reconstruct the induced field: this obviates the need to deconvolve the reference field but it introduces an additional bias. The dotted error ellipses introduce a large electrode configuration using the interior surface of the balloon for improved measurement accuracy (see Appendix).

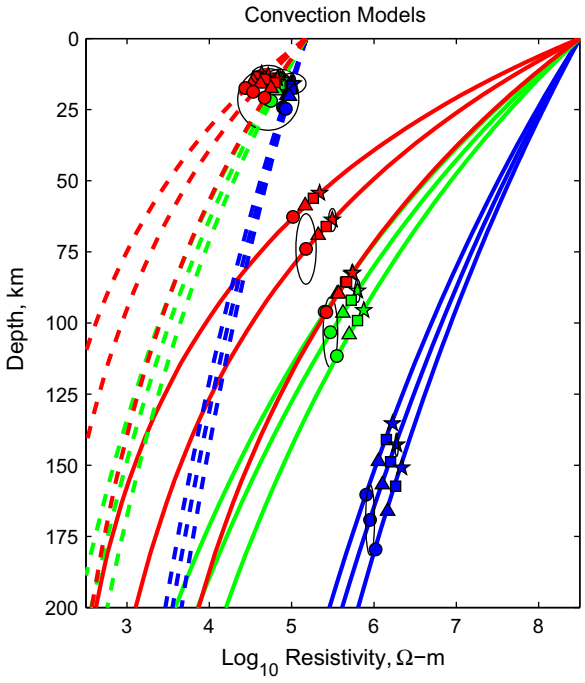

Fig. 8. Point soundings for convection models. Red, green, and blue correspond to Rayleigh numbers = 10^4, $\sim 10^3$, and 10^2, respectively. Error ellipses are for nominal measurement. The selected profiles for each model are representative of the mean and standard deviation but are actual. Compare to Fig. 5. (For interpretation of the references to color in this figure legend, the reader is referred to the web version of this article.)

plots representative resistivity-depth curves for wet and dry olivine for the three convection models ($Ra = 10^2$, $\sim 10^3$, and 10^4). These are individual points from the model but were chosen to be representative of the mean plus/minus one standard deviation. Note that the variability increases as Ra increases and $\overline{L}$ thins. The reference model (Fig. 8) again shows good recovery for dry olivine and poor results for wet olivine. The crust (Fig. 9) has no effect on

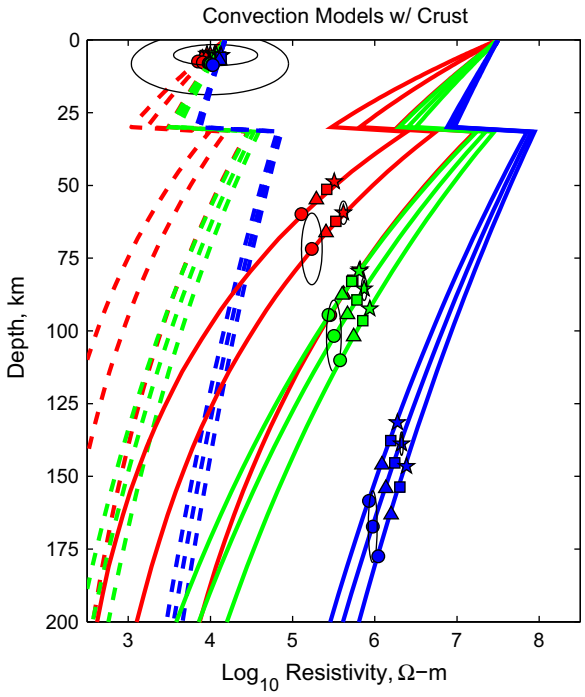

Fig. 9. Point soundings for convection models with conductive crust superimposed. Compare to Fig. 6.

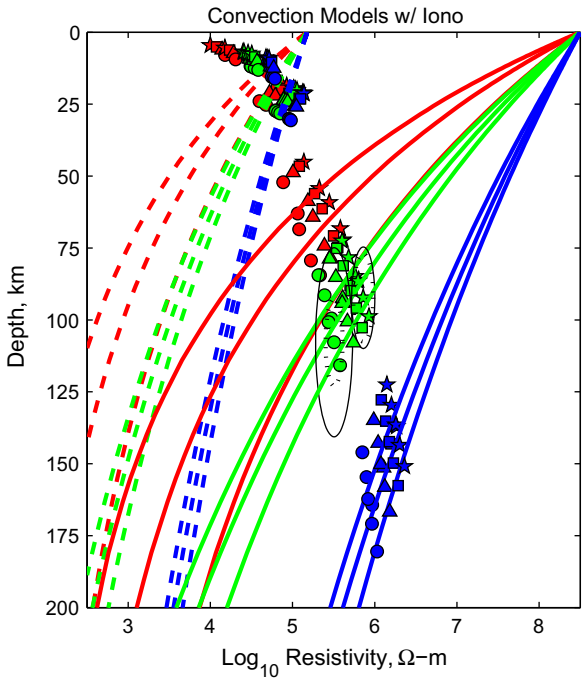

Fig. 10. Point soundings for convection models with aerial-measurement effects (ionosphere and quadrature bias). Large errors for wet ground conductivities not shown. Compare to Fig. 7.

Table 1
Point measurement accuracy of lithospheric thermal gradient.

Mantle conductivity	Dry	Dry	Dry	Dry	Wet	Wet	Wet	Wet
Ionosphere error?	No	Yes	No	Yes	No	Yes	No	Yes
Conductive crust?	No	No	Yes	Yes	No	No	Yes	Yes
True dT/dz, K/km (L, km)	Inferred dT/dz and standard error							
9.5 (100)	9.5 ± 5.8 (2.4)	7.1 ± 39 (13)	4.0 ± 37 (37)	NR	8.4 ± 13 (2.0)	NR	9.4 ± 29 (2.2)	NR
4.8 (200)	5.0 ± 2.0 (1.1)	5.2 ± 6.6 (3.9)	4.7 ± 3.2 (2.8)	4.5 ± 8.2 (7.2)	4.6 ± 5.2 (0.7)	NR	4.6 ± 43 (41)	NR
3.2 (300)	3.3 ± 1.1 (0.7)	3.4 ± 3.2 (1.9)	3.3 ± 1.1 (0.6)	3.3 ± 3.6 (2.8)	3.1 ± 3.1 (0.4)	NR	NR	NR
2.4 (400)	2.5 ± 0.7 (0.5)	2.6 ± 1.9 (1.2)	2.5 ± 0.7 (0.4)	2.4 ± 2.1 (1.7)	2.3 ± 2.2 (0.3)	NR	NR	NR
1.9 (500)	2.0 ± 0.5 (0.4)	2.1 ± 1.3 (0.9)	2.0 ± 0.5 (0.3)	2.0 ± 1.4 (1.2)	1.8 ± 1.7 (0.3)	NR	NR	NR

L = Lithospheric thickness: uniform thermal gradient from 740 to 1690 K over depth L.
NR = no result (failed inversion or extreme error).
Errors reported for nominal electrometer; numbers in parentheses use optimal electrometer.

Table 2
Ensemble measurement accuracy of lithospheric thermal gradient.

Mantle conductivity	Dry	Dry	Dry	Dry	Wet	Wet	Wet	Wet
Ionosphere error?	No	Yes	No	Yes	No	Yes	No	Yes
Conductive crust?	No	No	Yes	Yes	No	No	Yes	Yes
True dT/dz, Std. Dev., K/km	Inferred dT/dz and standard error							
4.1 ± 1.0 ($Ra = 10^4$)	4.3 ± 1.0	4.6 ± 1.1	4.1 ± 0.9	3.9 ± 0.8	4.0 ± 1.1	5.1 ± NR	4.5 ± 0.5	NR
2.6 ± 0.4 ($Ra \cong 10^3$)	2.8 ± 0.3	2.9 ± 0.3	2.8 ± 0.3	2.8 ± 0.3	2.6 ± 0.3	3.4 ± NR	4.1 ± 0.1	NR
1.2 ± 0.1 ($Ra = 10^2$)	1.4 ± 0.1	1.4 ± 0.1	1.4 ± 0.1	1.4 ± 0.1	1.3 ± 0.1	2.0 ± NR	5.2 ± 0.1	NR

Ra = Rayleigh number.
NR = no result (failed inversion or extreme error).

these models (because the thinnest $\bar{L} = 250$ km). The aerial measurement (Fig. 10) for wet olivine again fails to provide useful inferences about $\bar{L}$. Even with bias and the small electrometer, these cases can be distinguished for dry olivine.

Such interpretation of Figs. 8–10 still treats the results as point measurements. We are interested in comparing these point estimates to the large-scale lateral averages afforded by the convection models. Tables 1 and 2 give the geothermal gradients for each of the lithospheric models used in this paper (actual for specified lithospheres, mean for convection models) and the estimated values and errors from Section 3.7. These results also span all 8 combinations of conductivity law and effect of crust or ionosphere. The best-case accuracies for the reference point measurements in the range of expected lithospheric thicknesses for Venus are 20–30%. However, the accuracy on thermal gradient degrades to ~100% or worse when the airborne measurement is treated. The 513 grid points in the convection models provide an equal number of measurement stations, so the average thermal gradient on the profile can be improved by averaging. We find that for all cases with dry olivine, the standard deviation of the estimated thermal gradient is comparable to the standard deviation of the data, <25%. The nominal electrometer is sufficient for this purpose. The difficulties in measuring the small electric fields induced in wet olivine preclude assessment of errors on thermal gradient and in the worst cases no estimate is obtained at all.

The standard deviation of the mean estimated thermal gradient is of course smaller by $\sqrt{513}$, in which case the net error on geothermal gradient is dominated by the bias or offset between the estimated and true values, typically ~10% in Table 2.

5. Concluding discussion

We have developed a comprehensive, but still exploratory, conceptual framework for EM sounding of the lithosphere of Venus. We found that lightning-caused Schumann resonances are capable of penetrating 50–100 km in a dry Venus, thus investigating a depth interval sensitive to vertical temperature changes. This allows estimation of lithospheric thickness or thermal gradient. The presence of hundreds of ppm H_2O will increase conductivity enough so that the vertical length scale is limited to <20 km. This, and the decrease in measurement SNR, precludes robust estimation of lithospheric properties. The presence of significant water in the crust of Venus could nonetheless be inferred, and variations in shallow structure tracked.

The higher SNR in a three-component electrometer composed of orthogonal booms is superior to using a two-component electrometer and a magnetometer. Even if the vertical electrode separation is restricted to ~1 m, the SNR in measuring the vertical electric field as the reference is still much greater than using the horizontal magnetic field. A large electrode area and tip separation are important for obtaining good measurements of the horizontal electric field. Using the balloon itself is the optimal solution to obtaining high E-field SNR (Appendix).

We have shown that aerial EM sounding on Venus is really a joint investigation of the subsurface and ionosphere. With long traverses (~10^4 km), mean properties of the ionosphere and subsurface can be recovered. Joint regional (~10^3 km) inversion may be possible with additional constraints, e.g., the variation of the ionospheric resistivity with SZA and recognition that the ground resistivity will be correlated at long wavelength with topography (both are correlated with temperature). Local (~10^2 km) solutions (essentially point measurements) may provide useful tiepoints if the ionospheric resistivity can be estimated from distortion in the balloon downlink.

The data processing follows the usual hierarchy, with associated increasing sophistication of interpretation. The complex spectra form the Level 1 data (likely available data rates from a balloon will not permit return of raw time series: onboard spectral estimation is necessary). Solution of EM measurements for resistivity vs. depth forms Level 2 data. Such data are useful for confirming the predicted vertical and horizontal trends expected for the increase of temperature with depth and the larger thermal anomalies over volcanic rises. Thickened crust over plateau (tessera) highlands would also be evident. Level 3 data follow from the final step described here, estimation of thermal gradient.

The electric-field measurements required for aerial EM sounding on Venus are closely related to those used in space- and atmo-

spheric-physics investigations, onboard processing can return compact but useful data, and long traverses can separate ground and ionospheric contributions. The general approach described can be implemented for high-altitude (20 km) surveying on Earth and ionospheric conductivity can be estimated from GPS-signal delay. If Mars or Titan have lightning, they too will likely have Schumann resonances, and can be electromagnetically probed from aerial vehicles.

Acknowledgments

This research was supported by SwRI IR&D Project R8043 and by NASA Grant NNX07AP27G. We are grateful to two anonymous reviewers, one of whom substantially changed the trajectory of the paper by pointing out more recent experiments on the conductivity of hydrous olivine.

Appendix A. Spherical-octant electrode configuration

We have developed a novel electrode design suitable for wave-tilt measurements from a balloon. All "electrically small" measurements depend critically on two parameters: the capacitive reactance Z of the sensors and their "effective" separation Δx. Because $Z = 1/\omega C$, where ω is the angular frequency and C is the capacitance, it is essential to increase capacitance as frequency is decreased in order to maintain a given noise level in the amplifier. C is nearly a linear function of electrode size. The signal ΔV increases linearly with Δx (because $E \cong \Delta V/\Delta x$). Therefore the signal-to-noise ratio (SNR) increases with C and Δx.

Prior aerial electric-field measurements have used parallel or curved plates, small spheres or cylinders separated by booms, or limited surfaces on a sphere. Each of these geometries has a drawback in small capacitance, small effective separation, or inability to measure three spatial components of the electric field.

Our electrode array (Fig. A1) is nearly optimal for low-frequency balloon measurements, in that it:

1. Is a minimum-volume configuration by using the surface of a sphere.
2. Maximizes capacitance by using nearly 50% of the available surface area.
3. Maximizes electrode separation by differencing voltages across opposing hemispheres (the small separations at the corners have little effect because the affected area is small).
4. Is able to measure three spatial components of the field by alternately joining pairs of electrodes and differencing them with the opposing pair. In this way only four electrodes are required where normally six would be used.

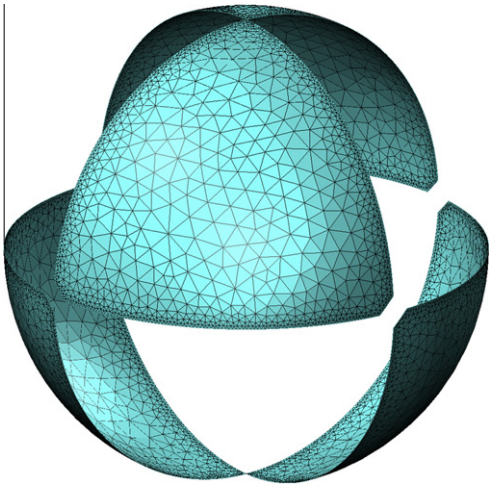

Fig. A1. Spherical octant electrode design for aerial E-field measurement. By alternately joining the electrodes in pairs and differencing with the complementary pair, three spatial components are recovered. This configuration maximizes capacitance and effective antenna length and minimizes volume and self-interference. Computational mesh is superimposed.

Through numerical modeling, we determined that $C \cong 76a$ pF and $\Delta x \cong 0.7a$, where a is the sphere radius in meters. These relations assume the corner gap is $\ll a$. There are several additional benefits to this design that optimize its incorporation into a balloon hull:

5. The electrodes can be sufficiently thin so as not to substantially impact balloon mass.
6. The electrode flexibility and configuration along the gore direction will make them easy to build into the balloon hull and not affect deployment or flight performance.
7. The cable bundle containing the attachment leads running from the top to bottom of the balloon can be incorporated with existing structural/signal lines. The entire line can be actively driven to make it electrically "invisible."

The voltages on the individual electrodes must be amplified and differenced (and digitized) to produce an E-field measurement. We have designed the relevant circuitry based on the OPA129 op-amp. For a 6-m balloon, the predicted sensitivity at 10 Hz is better than 50 pV/m/$\sqrt{}$Hz.

We note finally that the measurements claimed in a 2004 US patent by Barringer (#6,765,383) at frequencies less than hundreds of hertz (indeed, down to <1 Hz) are physically impossible due to the small size and spacing of the electrodes.

References

Arcone, S., 1978. Investigation of a VLF airborne resistivity survey conducted in northern Maine. Geophysics 43, 1399–1417.
Arkani-Hamed, J., 1994. On the thermal evolution of Venus. J. Geophys. Res. 99, 2019–2033.
Barringer, A.R., 1973. Geophysical exploration method using the vertical electric components of a VLF field as a reference, U.S. Patent, Nr. 3594,633.
Bevington, P.R., 1969. Data Reduction and Error Analysis for the Physical Sciences. McGraw-Hill, New York, 336pp.
Bolfan-Casanova, N., 2005. Water in the Earth's mantle. Mineral. Mag. 69, 229–257.
Borucki, W.J. et al., 1982. Predicted electrical conductivity between 0 and 80 km in the venusian atmosphere. Icarus 51, 302–321.
Bostick, F.X., 1977. A simple almost exact method of magnetotelluric data analysis. Proc. Workshop on Electrical Methods in Geothermal Exploration, Univ. Utah.
Brace, L.H., Kliore, A.J., 1991. The structure of the Venus ionosphere. Space Sci. Rev. 55, 81.
Brace, L., Elphic, R., Curtis, S., Russell, C., 1983. Wave structure in the Venus ionosphere downstream of the terminator. Geophys. Res. Lett. 10, 1116–1119.
Bullock, M.A. et al., 2009. Venus flagship mission study: Report of the Venus science and technology definition team. JPL.
Constable, S., 1993. Constraints on mantle electrical conductivity from field and laboratory measurements. J. Geomag. Geoelectr. 45, 707–728.
Constable, S., Shankland, T.J., Duba, A., 1992. The electrical conductivity of an isotropic olivine mantle. J. Geophys. Res. 97, 3397–3404.
Egbert, G.D., Booker, J.R., 1992. Very long period magnetotellurics at Tucson Observatory: Implications for mantle conductivity. J. Geophys. Res. 97, 15099–15112.
Grebowsky, J.M., Strangeway, R.J., Hunten, D.M., 1997. Evidence for Venus lightning. In: Boucher, S.W. et al. (Eds.), Venus II. Univ. Arizona Press, Tucson, pp. 125–157.
Grimm, R.E., 2002. Low-frequency electromagnetic exploration for groundwater on Mars. J. Geophys. Res. 107. doi:10.1029/2001JE001504.
Grimm, R.E., 2009. Electromagnetic sounding of solid planets and satellites. NRC White Paper. <www8.nationalacademies.org/ssbsurvey/publicview.aspx>.
Grimm, R.E., Hess, P.C., 1997. The crust of Venus. In: Boucher, S.W. et al. (Eds.), Venus II. Univ. Arizona Press, Tucson, pp. 1205–1244.
Grinspoon, D.H., 1993. Implications of the high D/H ratio for the sources of water in Venus' atmosphere. Nature 363, 428–431.
Jones, A.G., Ferguson, I.J., 2001. The electric Moho. Nature 409, 331–333.

Karato, S., 2006. Remote sensing of hydrogen in the Earth's mantle. Rev. Mineral. Geochem. 62, 343–375.
Kaula, W.M., Phillips, R.J., 1981. Quantitative tests for plate tectonics on Venus. Geophys. Res. Lett. 8, 1187–1190.
Lizarralde, D., Chave, A., Hirth, G., Schultz, A., 1995. Northeastern pacific mantle conductivity profile from long-period magnetotelluric sounding using Hawaii-to-California submarine cable data. J. Geophys. Res. 100, 17837–17854.
Lognonné, P., Occhipinti, G., Garcia, R., 2005. Seismic interior/atmosphere coupling on Venus. Lunar Planet. Sci. XXXVI. Abstract 2274.
McNeill, J.D., 1990. Use of electromagnetic methods for groundwater studies. In: Ward, S.H. (Ed.), Geotechnical and Environmental Geophysics, vol. 1. Society of Exploration Geophysicists, Tulsa, pp. 191–218.
McNeill, J.D., Labson, V.F., 1991. Geological mapping using VLF radio fields. In: Nabighian, M.N. (Ed.), Electromagnetic Methods in Applied Geophysics, vol. 2. Society of Exploration Geophysicists, Tulsa, pp. 521–640.
Moore, W.B., Schubert, G., 1997. Venusian crustal and lithospheric properties from nonlinear regressions of highland geoid and topography. Icarus 128, 415–428.
Moresi, L.-N., Solomatov, V.S., 1995. Numerical investigation of 2D convection with extremely large viscosity variations. Phys. Fluids 7, 2154–2162.
Namiki, N., Solomon, S.C., 1995. Degassing of argon, helium, and water and the nature of crustal formation on Venus. Lunar. Planet. Sci. XXVI, 1029–1030 (abstract).
Nickolaenko, A.P., Hayakawa, M., 2002. Resonances in the Earth-Ionosphere Cavity. Kluwer, Dordrecht, 380pp.
Nickolaenko, A.P., Rabinowicz, L.M., 1982. On the possibility of existence of global electromagnetic resonances on the planets of the Solar System. Space Res. 20, 82–89.
Pechony, O., Price, C., 2004. Schumann resonance parameters calculated with a partially uniform knee model on Earth, Venus, Mars, and Titan. Radio Sci. 39. doi:10.1029/ 2004RS003056.
Phillips, R.J., Malin, M.C., 1983. The interior of Venus and tectonic implications. In: Hunten, D.M. et al. (Eds.), Venus. Univ. Arizona Press, pp. 159–214.
Phillips, R.J. et al., 1997. Lithospheric mechanics and dynamics on Venus. In: Boucher, S.W. et al. (Eds.), Venus II. Univ. Arizona Press, Tucson, pp. 1163–1204.
Poe, B.T., Romano, C., Nestola, F., Smyth, J.R., 2010. Electrical conductivity anisotropy of dry and hydrous olivine at 8 GPa. Phys. Earth Planet. Inter. 181, 103–111.
Roux, A. et al., 2008. The search coil magnetometer for THEMIS. Space Sci. Rev. 141, 265–275.
Russell, C.T. et al., 2007. Lightning on Venus inferred from whistler-mode waves in the ionosphere. Nature 450, 661–662.
Russell, C.T., Zhang, T.L., Wei, H.Y., 2008. Whistler mode waves from lightning on Venus: Magnetic control of ionospheric access. J. Geophys. Res. 113. doi:10.1029/2008JE003137.
Sagdeev, R.Z., Linkin, V.M., Blamont, J.E., Preston, R.A., 1986. The VEGA Venus balloon experiment. Science 231, 1407–1408.
Schubert, G., Solomatov, V.S., Tackley, P.J., Turcotte, D.L., 1997. In: Boucher, S.W. et al. (Eds.), Venus II. Univ. Arizona Press, Tucson, pp. 1245–1287.
Schubert, G., Turcotte, D.L., Olson, P., 2001. Mantle convection in the Earth and planets. Cambridge Univ. Press, 940pp.
Simões, F. et al., 2008. Electromagnetic wave propagation in the surface-ionosphere cavity of Venus. J. Geophys. Res. 113. doi:10.1029/2007JE003045.
Simpson, F., Bahr, K., 2005. Practical Magnetotellurics. Cambridge Univ. Press, 254pp.
Sjogren, W.L. et al., 1997. The Venus gravity field and other geodetic parameters. In: Boucher, S.W. et al. (Eds.), Venus II. Univ. Arizona Press, Tucson, pp. 1125–1161.
Solomatov, S., 1995. Scaling of temperature- and stress-dependent viscosity convection. Phys. Fluids 7, 266–274.
Solomatov, V.S., Moresi, L.-N., 1996. Stagnant lid convection on Venus. J. Geophys. Res. 101, 4737–4753.
Solomon, S.C., Head, J.W., 1982. Mechanisms for lithospheric heat transport on Venus: Implications for tectonic style and volcanism. J. Geophys. Res. 87, 9236–9246.
Solomon, S.C. et al., 1992. Venus tectonics: An overview of Magellan observations. J. Geophys. Res. 97, 13199–13255.
Telford, W.M., Geldart, L.P., Sheriff, R.E., 1990. Applied Geophysics, second ed. Cambridge Univ. Press, 770pp.
Turcotte, D.L., 1993. An episodic hypothesis for venusian tectonics. J. Geophys. Res. 98, 17061–17068.
Turcotte, D.L., 1995. How does Venus lose heat? J. Geophys. Res. 100, 16931–16940.
Vozoff, K., 1991. The magnetotelluric method. In: Nabighian, M.N. (Ed.), Electromagnetic Methods in Applied Geophysics, vol. 2. Society of Exploration Geophysicists, Tulsa, pp. 641–711.
Wait, J.R., 1970. Electromagnetic waves in stratified media, Pergamon.
Wang, D., Mookherjee, M., Xu, Y., Karato, S., 2006. The effect of water on the electrical conductivity of olivine. Nature 443, 977–980.
Wight, D.E., Bostick, F.X., 1980. Cascade decimation – A technique for the real time estimation of power spectra. IEEE Int'l Conf. Acoustic Speech and Signal Proc., pp. 626–629.
Wilson, C.F. et al., 2011. The 2010 European Venus Explorer (EVE) mission proposal: The first in situ circumnavigation of an alien world. Exp. Astron., submitted for publication.
Wittall, K.P., Oldenburg, D.W., 1992. Inversion of magnetotelluric data for a one-dimensional conductivity. Geophys. Monogr. Ser. 5. Society of Exploration Geophysicists, Tulsa, 114pp.
Xu, Y., Shankland, T.J., Poe, B.T., 2000. Laboratory-based electrical conductivity in the Earth's mantle. J. Geophys. Res. 105, 27865–27875.
Yoshino, T., Matsuzaki, T., Shatskiy, A., Katsura, T., 2009. The effect of water on the electrical conductivity of olivine aggregates and its implications for the electrical structure of the upper mantle. Earth Planet. Sci. Lett. 288, 291–300.